

Development of Wear-Resistant Cu-10Cr-3Ag Electrical Contacts with Nano-Al₂O₃ Dispersion by Mechanical Alloying and High Pressure Sintering

S. BERA, W. LOJKOWSKY, and I. MANNA

Cu-10Cr-3Ag (wt pct) alloy with nanocrystalline Al₂O₃ dispersion was prepared by mechanical alloying and consolidated by high pressure sintering at different temperatures. Characterization by X-ray diffraction and scanning electron microscopy or transmission electron microscopy shows the formation of nanocrystalline matrix grains of about 40 nm after 25 hours of milling with nanometric (<20 nm) Al₂O₃ particles dispersed in it. After consolidation by high pressure sintering (8 GPa at 400 °C to 800 °C), the dispersoids retain their ultrafine size and uniform distribution, while the alloyed matrix undergoes significant grain growth. The hardness and wear resistance of the pellets increase significantly with the addition of nano-Al₂O₃ particles. The electrical conductivity of the pellets without and with nano-Al₂O₃ dispersion is about 30 pct IACS (international annealing copper standard) and 25 pct IACS, respectively. Thus, mechanical alloying followed by high pressure sintering seems a potential route for developing nano-Al₂O₃ dispersed Cu-Cr-Ag alloy for heavy duty electrical contact.

DOI: 10.1007/s11661-009-0019-7

© The Minerals, Metals & Materials Society and ASM International 2009

I. INTRODUCTION

IN the past, several studies have been conducted to enhance the mechanical strength of Cu alloys either through solid solution and precipitation strengthening by addition of an appropriate solute element whose solid solubility decreases with lowering of temperature (say, Cr, Ag, Nb, Zr, or Ta) or by dispersing insoluble oxides/ceramics to form metal-matrix composites.^[1–16] Precipitation or age hardening of these alloys produces fine coherent precipitates that provide the necessary strength in Cu alloys. Furthermore, strength and hardness of the matrix phase may increase with a decrease in grain size following the Hall–Petch relationship.^[17] Correia *et al.*^[18] achieved both precipitation and dispersion hardening in water-atomized and warm-extruded Cu-Cr and Cu-Cr-Zr alloy powders and carried out suitable microstructural characterization and mechanical property evaluation. A number of other investigations with Cu-Cr based alloys have studied the crystal structure of the metastable coherent precipitates^[19–22] and their influence on the tribological performance,^[22–24] thermal stability,^[25] oxidation behavior,^[26] and mechanical properties^[24,27] of these alloys. Besides alloying, ceramic oxide dispersion in the Cu matrix is known to improve mechanical properties of Cu alloys and enable retention of strength at high temperature

generated during use (*i.e.*, Joule heating, friction, and wear).^[28–32]

Nanometric materials are characterized by a unique microstructure comprising ultrafine crystallites/domains and very high specific surface/interfacial area of the crystallites that account for a host of novel properties not feasible in their coarse-grained counterparts.^[33,34] Siegel^[33] compared this microstructural state of having an almost equal number of atoms constituting nanometric crystallites and very high surface/volume fraction of interfaces/interfacial regions with “bimodal” distribution of grain body and boundary phases. Several nonequilibrium processes may generate the aforementioned nanostructured alloys or nano-oxide dispersed metal-matrix composites. Among these routes, mechanical alloying is one of most convenient, flexible, and inexpensive methods of producing nanostructured materials from elemental powder blends.^[35,36] The main advantage of this advanced powder metallurgy process lies in faster kinetics, grain refinement, extension of solid solubility, and development of a novel composite aggregate comprising uniform dispersion of dissimilar/incoherent/insoluble phases, in nanocrystalline/amorphous matrix. It is relevant to point out that the scope of developing nanoceramic/intermetallic phase dispersed extended solid solution of Cu-Cr/Cu-Cr-Ag by mechanical alloying has not been explored/reported in the past.

The present investigation aims to synthesize Cu-10Cr-3Ag (wt pct) alloy powders by mechanical alloying, obtain homogeneous dispersion of nanoceramic Al₂O₃ particle in the alloyed matrix by subsequent mechanical milling, and then consolidate the product into bulk solid component by high pressure sintering for microstructural characterization and assessment of physical, mechanical, and electrical properties of the compacts.

S. BERA, Doctoral Student, and I. MANNA, Professor, are with the Metallurgical and Materials Engineering Department, Indian Institute of Technology, Kharagpur, W.B. 721302, India. Contact e-mail: imanna@metal.iitkgp.ernet.in W. LOJKOWSKY, Professor, is with the Polish Academy of Sciences, Institute of High Pressure Physics (UNIPRESS), Warszawa 01-142, Poland.

Manuscript submitted January 10, 2009.

Article published online October 27, 2009

II. EXPERIMENTAL

Appropriate amounts of Cu, Cr, and Ag elemental powders (with each constituent having at least 99.5 wt pct purity and about 50- to 100- μm particle size) were subjected to mechanical alloying in a Retsch PM 400 high-energy planetary ball mill operated at 300 rpm with 10:1 ball to powder weight ratio using stainless steel vial and balls (10-mm diameter) to yield single-phase Cu-Cr-Ag product with some undissolved Cr (dispersed in the single-phase Cu-Cr-Ag solid solution matrix). Nanocrystalline Al_2O_3 powder (Inframat Advanced Materials, Farmington, CT) was dispersed to 5 wt pct in a selected set of mechanically alloyed powder to effect homogeneous dispersion in the alloyed metallic matrix. Milling was done in wet (toluene) medium to prevent agglomeration of the powders and to retard oxidation beyond the initial stage of milling. The identity and sequence of phase evolution in different stages of mechanical alloying were studied by X-ray diffraction (XRD) using a Panalytical X'Pert Pro diffractometer with $\text{Co } K_\alpha$ (0.1789 nm) radiation.

At room temperature, the alloyed powder was compacted by 100 MPa pressure and then sintered at 400 °C, 600 °C, and 800 °C using high pressure compaction press at 8 GPa pressure using 4-mm-diameter graphite die with ceramic coating (BN). While pressure was gradually raised to 8 GPa, transient heating by a graphite susceptor lasted only for a minute. The samples were then allowed to cool to room temperature and stripped off the die for characterization. This transient heating at extremely high pressure yielded extremely dense samples. The microstructure of the compacted and sintered samples was studied using a scanning electron microscope (SEM) along with energy dispersive spectroscopy (EDS). Selected samples in the as-milled condition and high pressure sintered pellet form were studied by a JEOL* transmission electron microscope

*JEOL is a trademark of Japan Electron Optics Ltd., Tokyo.

(TEM) in the bright- or dark-field and high resolution lattice imaging mode.

The average hardness of the composite samples was measured with the help of a Vickers hardness tester at 0.5/1 N load from about 10 indentations at equivalent locations on the same sample. The density of the compacted and sintered samples was measured using Archimedes principle after weighing in air and in water separately using an electronic balance with a precision of 0.1 mg. Wear resistance of the pellets was studied by both ball-on-disc type of wear instrument and a fretting wear tester applying up to 20 N load with in a wear span of 1 mm and 10 Hz frequency and measuring the cumulative wear depth as a function of time. While ball-on-disc tests cover a wider area on the surface, fretting tests better simulate the frictional or abrasional wear encountered by copper-based electrical contacts. Therefore, both these types of common and popular wear testing methods were employed. The tests were conducted at ambient atmosphere without using any

lubricant. In both wear test methods, high pressure sintered disc-shaped samples (5 mm in diameter and 3 to 4 mm in height) were used. While a diamond tip was used to cause wear/scratch on the disc-shaped samples in the ball-on-disc method, the WC ball of 10-mm diameter was used during fretting wear test. The average surface roughness of the sintered samples was less than 0.1 μm . Electrical resistivity of the sintered pellets was measured at ambient temperature using the van der Pauw four-probe method^[37] with a high precision Keithley 2182A nano-voltmeter and 6220 current source (Keithley Instruments, Cleveland, OH).

III. RESULTS AND DISCUSSION

Figure 1(a) presents a series of XRD patterns showing phase evolution during mechanical alloying of Cu-10Cr-3Ag (wt pct) elemental powder blends as a function of cumulative milling time of 1 to 25 hours. Figure 1(b) shows similar XRD data revealing the phase aggregate in pellets prepared from these mechanically alloyed powders (25 hours) after blending with nanometric Al_2O_3 dispersion and sintering under high pressure (up to 8 GPa) at different temperatures (400 °C to 800 °C). It is evident that Cr and Ag

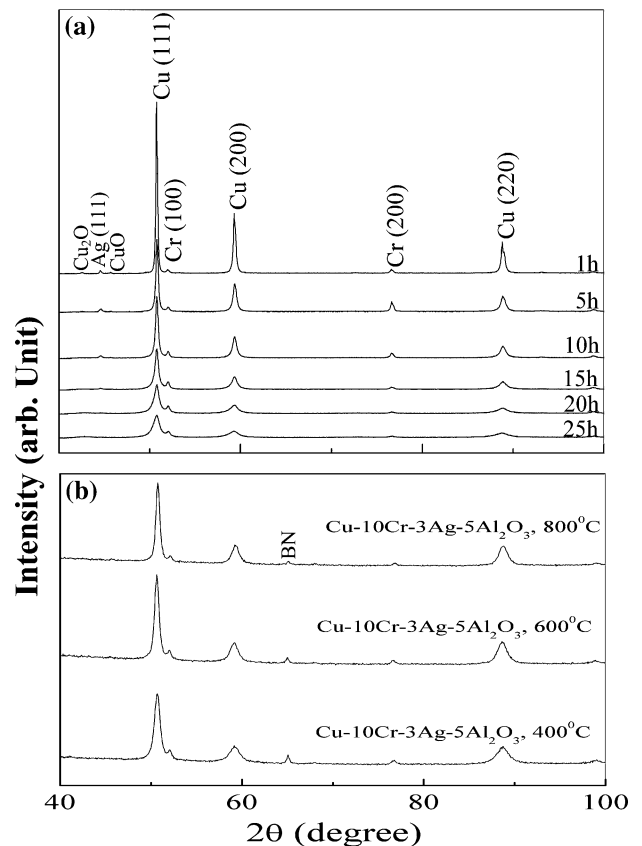


Fig. 1—XRD patterns of Cu-10Cr-3Ag (wt pct) after (a) mechanical alloying for cumulative time of 1 to 25 h and (b) consolidation of 25 h mechanically alloyed product by high pressure sintering at 400 °C, 600 °C, and 800 °C for 1 min, respectively.

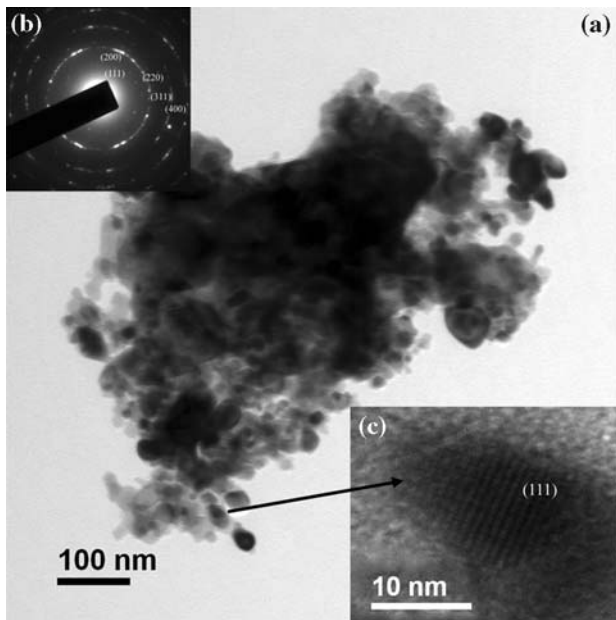


Fig. 2—(a) Bright-field TEM image of mechanically alloyed Cu-10Cr-3Ag powder after 25 h of milling, (b) SAD pattern of the powder showing a typical fcc ring pattern, and (c) a nanometric crystalline with (111) orientation.

dissolved in Cu during the course of mechanical alloying in a planetary ball mill to form a predominantly single-phase solid solution by about 20 hours. During the progress of milling, the peak width of the solid solution increases. The corresponding peak broadening analysis using Scherrer relation^[38] and applying appropriate corrections to eliminate errors due to strain and instrumental broadening^[39] shows that the crystallite size decreases to about 40 nm after 25 hours of milling. The XRD pattern (Figure 1(a)) shows that oxidation could not be avoided altogether during milling; however, the degree of oxidation is quite insignificant. In addition, the XRD pattern in Figure 1(b) shows that a small amount of impurity was picked up from the lubricant (boron nitride, indexed as BN) used during high pressure sintering. The phase aggregate is not truly a “single phase” as Cr peaks are detected in Figure 1(a). The bright-field TEM image of the alloy powder after 25 hours of milling (Figure 2) confirms the nano-metric size and distribution of the particles. A high resolution lattice image of one of these particles from the electron transparent edge shows an isolated (111) crystallite of about 15-nm average diameter. The bright-field image shows that all the particles are almost of identical dimension (about 40 nm in diameter), which is also comparable with the results obtained from the XRD data analysis. The corresponding ring-type SAD pattern confirms that the mechanically alloyed product is nanometric fcc solid solution with a lattice parameter of 0.3607 nm, which is slightly smaller than pure Cu (0.3615 nm). This difference can be attributed to the formation of Cu-Cr-Ag extended solid solution. Thus, mechanical alloying by high energy planetary ball milling seems effective to reduce the crystallite size to 40 nm from an initial particle size (of the elemental

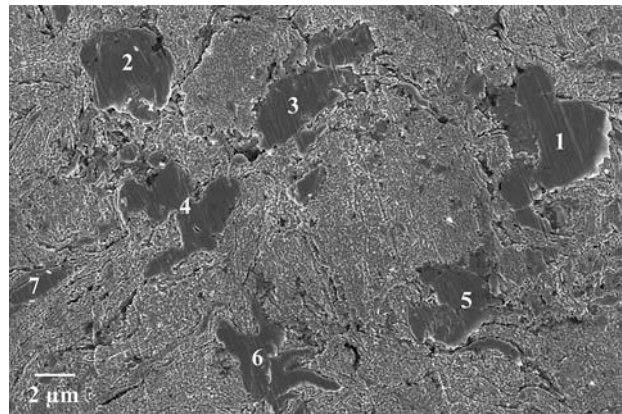


Fig. 3—SEM image of mechanically alloyed (for 25 h) and high pressure sintered (at 600 °C) Cu-10Cr-3Ag sample subjected to EDS spot analysis at different locations (1 through 7).

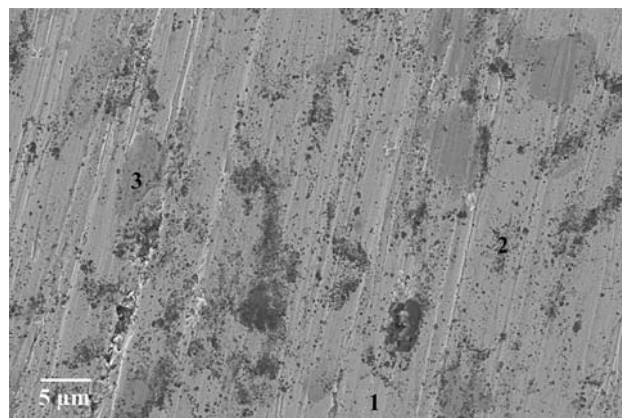


Fig. 4—Scanning electron micrograph of high pressure sintered (at 600 °C) 5 wt pct Al₂O₃ dispersed Cu-10Cr-3Ag composite. 1, 2, and 3 mark the EDS analysis spots.

powders) of 50 to 100 μm. It may be pointed out that reduction of crystallite size to a nanometric level is likely to aid in the extension of solid solubility (of Cr/Ag in Cu) due to the Gibbs–Thompson effect.^[40]

Figure 3 shows the SEM image of the high pressure sintered pellets of Cu-10Cr-3Ag alloy (without nano-Al₂O₃ dispersion) consolidated at 600 °C. The microstructure suggests that compaction by high pressure sintering produced uniform and dense compacts with a very few isolated pores of submicron size. The EDS analysis suggests that the dark regions (marked as 1 through 7) are Cr-rich spots arising possibly either from undissolved Cr retained from mechanical alloying or from precipitates formed during high pressure sintering at elevated temperature. The details of the EDS analysis are discussed later.

Figure 4 shows the effect of high pressure sintering on the microstructure of the same Cu-10Cr-3Ag blend with 5 wt pct nano-Al₂O₃ dispersion at the same (600 °C) temperature. The points marked 1 through 3 represent the locations of the EDS microanalysis to determine the local composition. The results of such elemental microanalysis are summarized in Table I. The bulk EDS

analysis (with a large area of analysis) shows that the composition is similar to that of the initial powder blend prior to milling. The presence of a negligible amount of Fe (<1 wt pct) indicates that the amount of impurity coming from the grinding medium during mechanical alloying is insignificant. The amount of Cr found in spots 1 and 2 is much lower than the quantity of Cr (10 wt pct) present in the initial powder blend. These are matrix regions partially depleted of Cr due to the precipitation of Cr-rich phases (Figure 4). In fact, the EDS analysis of spot 3 in Figure 4 records significantly higher (36.05 wt pct) Cr content, which implies that certain regions in the microstructure consist of Cr-rich precipitates in the forms of coarsened particles. Thus, the microstructure after sintering is not single phase anymore as Cr precipitates have been detected in the XRD pattern (Figure 1) as well as the SEM image (Figure 3 and point 3 in Figure 4). However, it may be noted that the EDS analysis of spots 1 and 2 in Figure 4 records the amount of Cr to be around 4 wt pct even after sintering. Therefore, it can be concluded that the matrix is an extended solid solution with a Cr content higher than its equilibrium solubility (of Cr in Cu).

These results are commensurate with the XRD analysis (Figure 1) of the milled powder and high pressure sintered pellets where a few isolated and low intensity Cr peaks have been detected. Although the entire amount of added elemental Cr does not dissolve in Cu, both bulk (wide area) and spot EDS analyses suggest that the entire amount of elemental Ag in the initial powder blend dissolves in the Cu-rich matrix. Furthermore, the EDS analysis at point 2 confirms the presence of Al₂O₃ nanoparticle in isolated locations in the Cu-10Cr-3Ag alloyed matrix.

Figure 5(a) shows the SEM image of the high pressure sintered pellet of Cu-10Cr-3Ag + 5 wt pct Al₂O₃ samples sintered at 800 °C. The inset (Figure 5(b)) shows the higher (150 k) magnification view of the selected area marked with a bright rectangle and reveals a few nano-Al₂O₃ dispersoids uniformly distributed in the Cu-rich matrix. A close observation reveals that this feature of uniform dispersion of ultrafine Al₂O₃ (100 to 200 nm) in the Cu-rich matrix is consistent throughout the microstructure and confirms that the present routine of mechanical alloying and high pressure sintering has been effective to produce a homogeneous nano-Al₂O₃ dispersed Cu-matrix composite. It is interesting to note that the interface of the nanometric Al₂O₃ particles with the matrix and regions around do not reveal any macro- or microdefect such as porosity or crack. Thus, it appears that the ceramic particles (dispersoids) have bonded well with the metallic matrix due to the combined effect of very high pressure (8 GPa) and high

temperature (400 °C to 800 °C) applied during sintering. This kind of strong bond between the dispersoid and matrix is essential in metal-matrix composites to prevent decohesion or fracture at the interface and ensure a maximum level of dispersion strengthening.

Figure 6 shows the microstructure and results of EDS line scan analysis on selected areas of a high pressure sintered Cu-10Cr-3Ag compact with 5 wt pct nano-Al₂O₃ dispersion consolidated at 800 °C. It is evident that Al, O₂, and Cr are concentrated in localized regions, while Ag is the only element distributed uniformly along the length of the line scan. The comparison of intensity distribution with distance suggests that Al and O₂ are present in the combined state at two locations separated by a few μm distance, and Cr is segregated in another region spread over 2 to 3 μm. This trend clearly suggests that nanometric Al₂O₃ particles are dispersed in separated regions and coarse Cr-rich particles are embedded in the matrix in isolated spots. Furthermore, the trend of the analysis related to Cr and Cu implies a significant interdiffusion between Cr and Cu. Therefore, it can be presumed that the embedded Cr particles form a strong and diffused bond with the Cu solid solution matrix.

Figure 7(a) shows the bright-field TEM image of 5 wt pct Al₂O₃ dispersed Cu-10Cr-3Ag alloy following high pressure sintering at 600 °C. It is evident that ultrafine Al₂O₃ is uniformly dispersed all over the Cu-base solid solution. The corresponding circular SAD pattern confirms that the matrix is an fcc solid solution (Figure 7(b)). The interplanar (*d*) spacing (0.343 nm), calculated from the corresponding lattice image (Figure 7(c)), is comparable to the *d* spacing of equilibrium

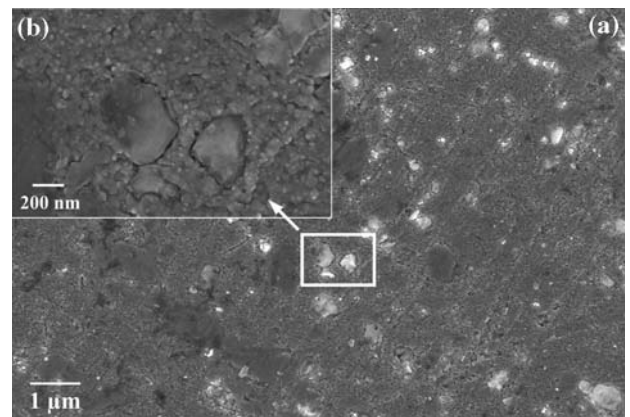


Fig. 5—(a) SEM image of Cu-10Cr-3Ag + 5Al₂O₃ sample after high pressure sintering at 800 °C. (b) Higher magnification (150 k) view of the selected region marked with a bright rectangle.

Table I. Summary of EDS Microanalysis at the Designated Locations Marked in Figure 4

Location	Cu (Wt Pct)	Cr (Wt Pct)	Ag (Wt Pct)	Al (Wt Pct)	O ₂ (Wt Pct)	Fe (Wt Pct)
Bulk	76.03	10.76	3.32	04.42	04.91	0.57
Point 1	88.21	04.77	3.19	01.67	01.8	0.35
Point 2	59.94	04.56	3.33	15.27	16.11	0.79
Point 3	51.31	36.05	1.51	03.94	06.83	0.36

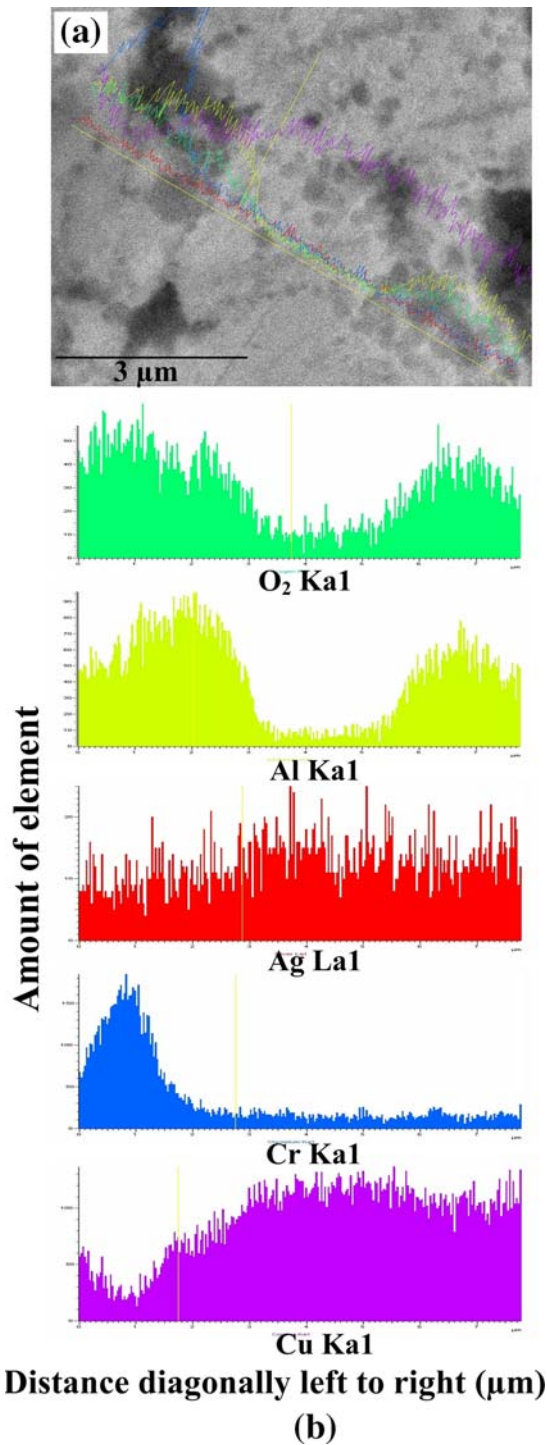


Fig. 6—(a) SEM image of 5 wt pct nano- Al_2O_3 dispersed Cu-10Cr-3Ag composite, high pressure sintered at 800 °C. (b) The results of elemental analysis per the line scan shown in (a).

synthetic corundum Al_2O_3 phase (0.348 nm, JCPDS data file, PDF No. 83-2080).

The physical, mechanical, and electrical properties of interest of the high pressure sintered pellets are summarized in Table II. While the density of the pellets with and without nano- Al_2O_3 sintered at 600 °C and 800 °C is comparable and around 8 Mg/m^3 , the hardness values

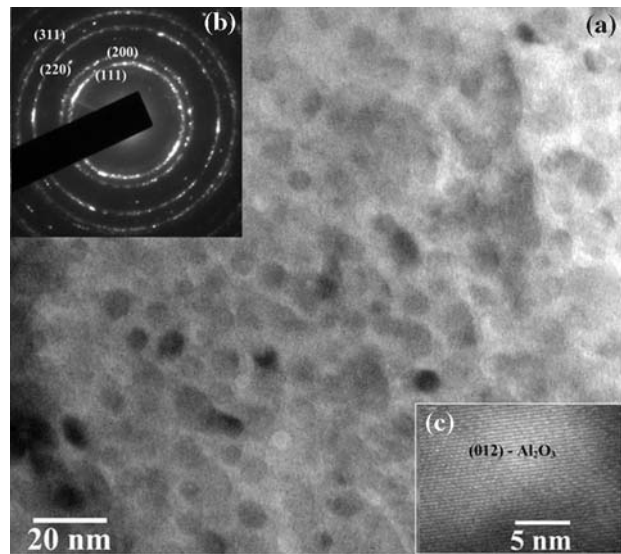


Fig. 7—(a) TEM image of 5 wt pct Al_2O_3 dispersed Cu-10Cr-3Ag alloy high pressure sintered at 600 °C. (b) The top left corner inset shows the SAD pattern from the fcc matrix. (c) The bottom right corner inset shows the lattice image of an isolated alumina particle.

of these pellets increase as the high pressure sintering temperature increases from 400 °C to 600 °C but decreases after sintering at a still higher temperature of 800 °C. The hardness value of the composites with 5 wt pct nano- Al_2O_3 dispersion is much higher than that of the base alloy under comparable conditions of processing or sintering. It may be noted that these hardness values with nano-alumina dispersion are significantly higher than those in the earlier reported studies on Cu-Cr alloys,^[18] Cu-Cr-Ag or Cu-Cr-Zr alloys,^[8,18,22,41] and nano- Al_2O_3 dispersed Cu matrix composite.^[30]

Figure 8 shows the kinetics of cumulative wear depth as a function of time in sintered pellets subjected to wear studies in a ball-on-disc type of wear instrument applying 20 N load. The wear depth of the sintered pellets is compared with that of the pure Cu block. It is evident that mechanically alloyed and high pressure sintered pellets record significantly higher resistance to wear than that of pure Cu block. The wear resistance increases with an increase in sintering temperature, though the highest resistance is recorded in the compact sintered at 600 °C, not 800 °C. This trend of better mechanical property at an intermediate (600 °C) temperature of sintering is similar to that recorded for hardness variation (Table II). Possibly, precipitation of Cr particles into the Cu matrix (Figure 1(b)) leads to the lowering of hardness and wear resistance following sintering at higher (800 °C) temperature.

Figure 9 shows the SEM image of the wear tracks or scar. Both the width and depth of the wear track of the hot-pressed pellets are much lower than those of the pure Cu block. The deep gouges formed in pure Cu block are absent in the sintered compacts. The damage is the minimum in the compact sintered at 600 °C. This minimal surface damage is commensurate with the

Table II. Summary of Relevant Physical, Electrical, and Mechanical Properties

System	Sintering Temperature (°C)	Density (mg/m ³)	Pct Theoretical Density	Resistivity (μΩ cm)	Conductivity (Pct IACS)	Hardness (VHN)
Cu-10Cr-3Ag	600	8.1	92	5.5	31	305 ± 5
	800	8.1	92	5.3	32	275 ± 5
Cu-10Cr-3Ag + 5Al ₂ O ₃	400	7.6	89	9.1	19	393 ± 5
	600	8.0	94	7.5	23	425 ± 5
	800	8.2	96	6.8	25	413 ± 5

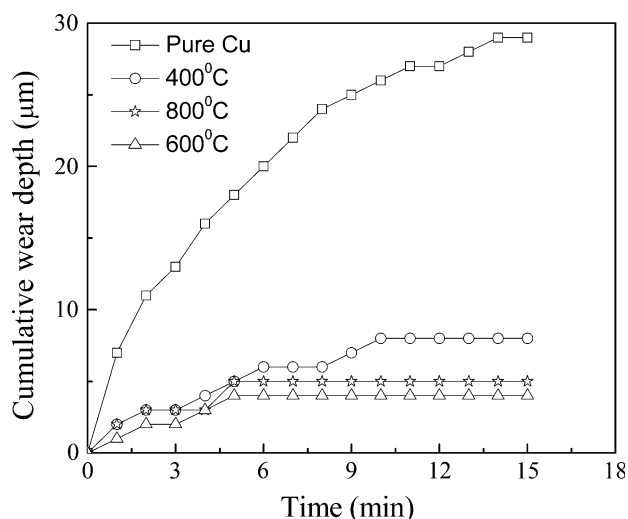


Fig. 8—Variation of cumulative wear depth as a function of time of pure Cu and Cu-10Cr-3Ag + 5Al₂O₃ pellets sintered at different temperatures.

earlier discussed trend of variation in hardness and wear damage with sintering temperature. Figure 10 shows the fretting wear depth as a function of cumulative time suffered by composites with different compositions after sintering at various temperatures. The addition of nanoceramic oxide increases the wear resistance of the composites to a significant extent. This also implies that the ceramic oxide particles form a good metallurgical bond with the metallic matrix that prevents pullout or ploughing of dispersoids. Between the two pellets with no ceramic oxide dispersion, the one sintered at 600 °C shows better wear resistance. Furthermore, among the pellets with 5 wt pct nano-Al₂O₃ dispersion, the pellet sintered at 600 °C shows the highest wear resistance in terms of wear depth. This is perhaps due to the fact that the degree of sintering is incomplete or poor at 400 °C, while the matrix undergoes substantial coarsening during sintering at 800 °C compared to that during sintering at lower (400 °C or 600 °C) temperature. The results of wear studies are in good agreement with the hardness values (Table II) and wear depth data of the respective compacts obtained from wear studies using ball-on-disc experiments (Figure 8).

The volume of the worn or fretted surface was calculated using the empirical equation used by Qu and Truhan.^[42] Figure 11 shows the calculated wear volume of different samples (1, 2, 3, 4, and 5 along the

axis of the abscissa represent Cu-10Cr-3Ag composites high pressure sintered at 600 °C and 800 °C and 5 wt pct Al₂O₃ dispersed Cu-10Cr-3Ag alloy hot pressed at 400 °C, 600 °C, and 800 °C, respectively). A typical wear scar developed in 5 wt pct nano-Al₂O₃ dispersed Cu-10Cr-3Ag composite sintered at 600 °C after fretting with 20 N load, 1-mm wear span, and 10 Hz frequency is shown in the inset. The Cu-10Cr-3Ag composite high pressure sintered at 800 °C is prone to maximum wear, while the 5 wt pct nano-Al₂O₃ dispersed Cu10Cr3Ag composite high pressure sintered at 600 °C and 800 °C registers almost comparable and the least wear volume among all the samples.

Since these composites are meant for electrical contacts or components, electrical resistivity of the sintered composites has been measured using the direct current van der Pauw four-probe method and is reported in Table II. The resistivity values of these composites are comparable to those of similar type of cast or wrought alloys reported in the literature.^[18,21,43,44] The Cu-10Cr-3Ag composite sintered at 800 °C shows the highest conductivity of 32 pct IACS (Table II). The pellets (without or with nano-Al₂O₃) sintered at 600 °C have lower conductivity than that of the pellets of similar composition sintered at 800 °C. This difference is attributed to a greater degree of grain coarsening (of the matrix) at higher sintering temperature. Thus, the amount of grain boundary and similar crystallite or macrodefects is less in the composites sintered at higher temperature. Consequently, the composites of similar composition sintered at higher temperature show lower resistivity or higher electrical conductivity. The 5 wt pct nano-Al₂O₃ dispersed Cu-10Cr-3Ag composite high pressure sintered at 800 °C shows a relatively lower conductivity of 25 pct IACS in comparison to that of 32 pct IACS of the composite with identical composition without nano-Al₂O₃ dispersion and sintered at the same (800 °C) temperature. It seems that nano-Al₂O₃ dispersion affects the conductivity, but the degree of increase in resistivity or decrease in conductivity is not severe. This may be due to the fact that the nanoceramic oxide particles are not coarsened during high-temperature pressing as the time of pressing is only 1 minute.

IV. CONCLUSIONS

Mechanical alloying of elemental Cu, Cr, and Ag powder in the weight ratio of Cu-10Cr-Ag in a planetary ball mill for 25 hours leads to formation of an extended

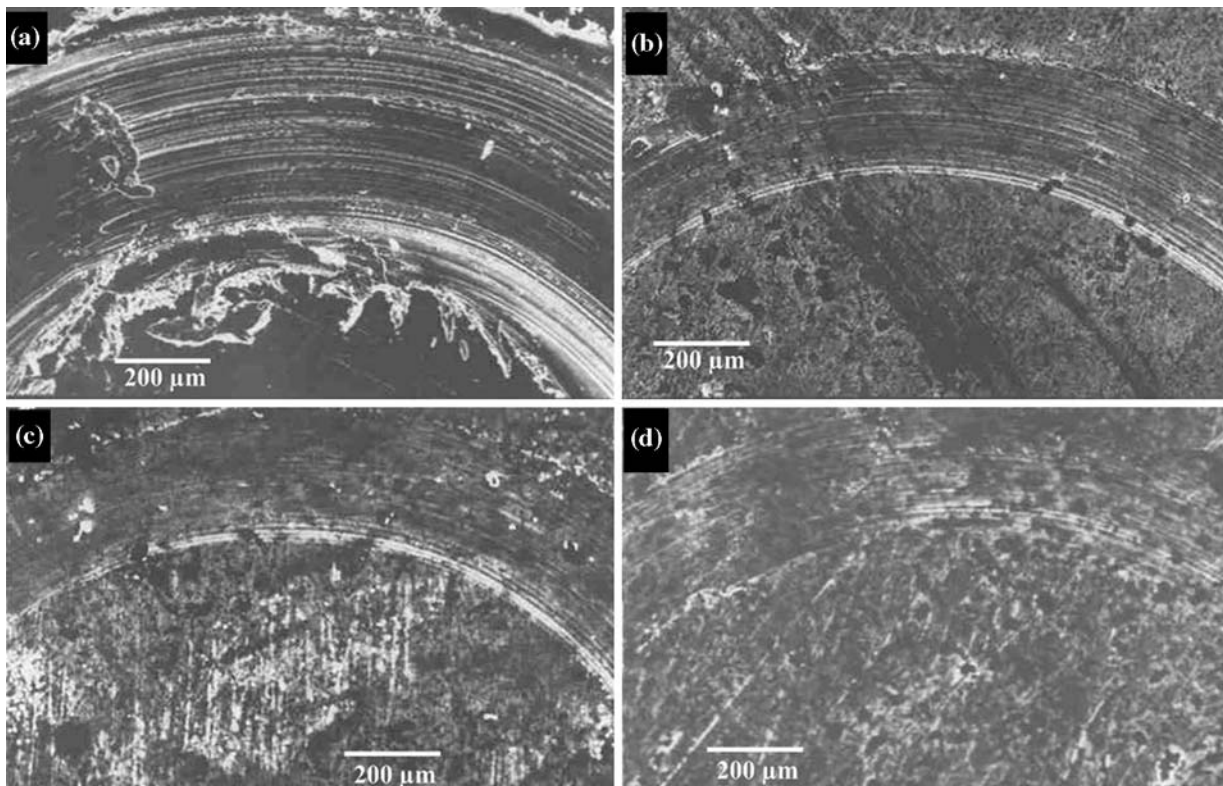


Fig. 9—SEM image of the wear scar or track suffered by the (a) Cu block and high pressure sintered Cu-10Cr-3Ag pellets with 5 wt pct Al_2O_3 consolidated at (b) 400 °C, (c) 600 °C, and (d) 800 °C.

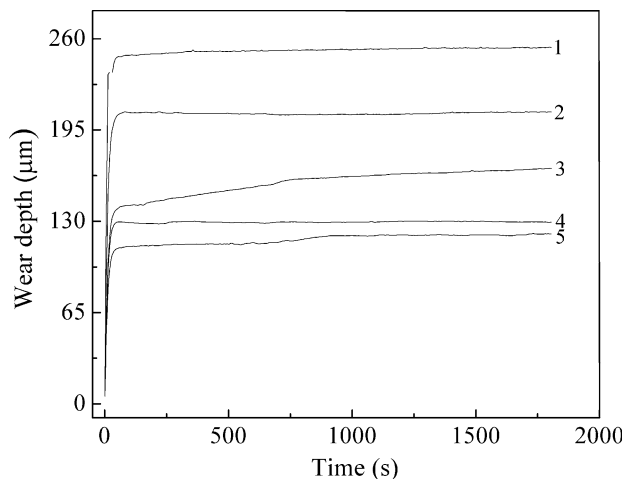


Fig. 10—Depth of fretting wear as a function of cumulative time for composites (with different compositions) sintered at various temperatures. Curves 1 and 2 are of Cu-10Cr-3Ag sintered at 800 °C and 600 °C, and curves 3, 4, and 5 are of 5 wt pct nano- Al_2O_3 dispersed Cu-10Cr-3Ag sintered at 400 °C, 800 °C, and 600 °C, respectively.

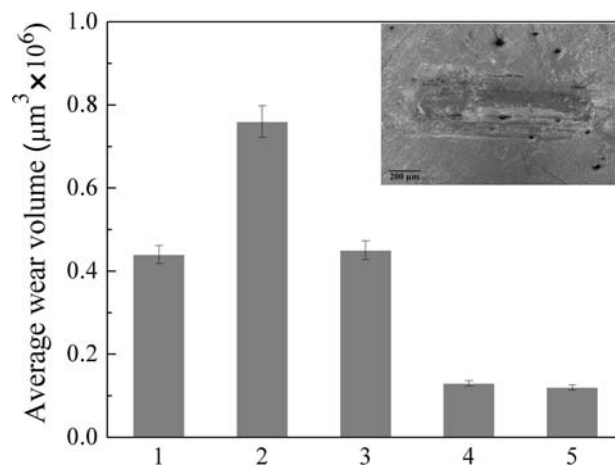


Fig. 11—Calculated wear volume of different samples (1, 2, 3, 4, and 5 along axis of abscissa represent Cu-10Cr-3Ag alloy sintered at 600 °C and 800 °C, and 5 wt pct nano- Al_2O_3 dispersed Cu-10Cr-3Ag alloy high pressure sintered at 400 °C, 600 °C, and 800 °C, respectively). The inset shows the wear scar developed in 5 wt pct nano- Al_2O_3 dispersed Cu-10Cr-3Ag alloy sintered at 600 °C after 1 h of fretting with 20 N load.

solid solution with a small amount of undissolved Cr in finely dispersed state. The TEM image confirms the XRD analysis result of crystallite size of 30 nm of the matrix phase after 25 hours of milling. High pressure (8 GPa) sintering at 400 °C to 800 °C for 1 minute is effective to form dense ($\sim 8.2 \text{ Mg/m}^3$) products. While

the matrix phase undergoes significant grain growth, the oxide dispersion does not undergo a noticeable change in the particle size after high pressure sintering at 400 °C, 600 °C, or 800 °C. While the hardness value of the composite without nanoceramic particle reinforcement is about 300 VHN, addition of 5 wt pct

nano-Al₂O₃ particle results an increase in hardness by about 35 pct (up to 425 VHN) and a significant improvement in wear resistance (reduction by a factor of 2 to 3) without adversely affecting the electrical conductivity (25 to 32 pct IACS) of the pellets.

ACKNOWLEDGMENTS

Partial financial support from the International Copper Association and Department of Science and Technology, New Delhi (Indo-Polish Project No. INT/POL/P-7/2004 and NSTI Grant No. SR/S5/NM-04/2005), is gratefully acknowledged. The authors sincerely appreciate the useful technical discussion with Professor J. Dutta Majumdar.

REFERENCES

- M.A. Morris and D.G. Morris: *Acta Metall.*, 1987, vol. 35, pp. 2511–22.
- D.G. Morris and M.A. Morris: *Mater. Sci. Eng.*, 1988, vol. 104, pp. 201–13.
- W.A. Spitzig and P.D. Krotz: *Acta Metall.*, 1988, vol. 36, pp. 1709–15.
- D.G. Morris, M.A. Morris, and J.C. Joye: *Mater. Sci. Eng. A*, 1992, vol. 58, pp. 111–17.
- M.A. Morris, M. Leboeuf, and D.G. Morris: *Mater. Sci. Eng. A*, 1994, vol. 188, pp. 255–65.
- F. Heringhaus, D. Raabe, and G. Gottstein: *Acta Metall.*, 1995, vol. 43, p. 1467.
- D. Raabe and U. Hangen: *Acta Metall.*, 1996, vol. 44, pp. 953–61.
- D. Raabe, K. Miyake, and H. Takahara: *Mater. Sci. Eng. A*, 2000, vol. 291, pp. 186–97.
- D. Raabe and J. Ge: *Scripta Mater.*, 2004, vol. 51, pp. 915–20.
- E. Botcharova, J. Freudenberger, and L. Schultz: *J. Alloys Compds.*, 2004, vol. 365, pp. 157–63.
- M.W. Decker, J.R. Groza, and J.C. Gibeling: *Mater. Sci. Eng. A*, 2004, vol. 369, pp. 101–11.
- L. Zhang and L. Meng: *Scripta Mater.*, 2005, vol. 52, pp. 1187–91.
- M. López, D. Corredor, C. Camurri, V. Vergara, and J. Jiménez: *Mater. Charact.*, 2005, vol. 55, pp. 252–62.
- S.G. Jia, M.S. Zheng, P. Liu, F.Z. Ren, B.H. Tian, G.S. Zhou, and H.F. Lou: *Mater. Sci. Eng. A*, 2006, vol. 419, pp. 8–11.
- E. Botcharova, J. Freudenberger, and L. Schultz: *Acta Mater.*, 2006, vol. 54, pp. 3333–41.
- W. Chen, Z. Kang, H. Shen, and B. Ding: *Rare Metals*, 2006, vol. 25, pp. 37–42.
- C. Meriç, E. Atik, and T. Engez: *Mater. Res. Bull.*, 1999, vol. 34, pp. 2043–52.
- J.B. Correia, H.A. Davies, and C.M. Sellar: *Acta Mater.*, 1997, vol. 45, pp. 177–90.
- K.J. Zeng and M. Himilinen: *J. Alloys Compds.*, 1995, vol. 220, pp. 53–61.
- K.B. Gerasimov, S.V. Mytnichenko, S.V. Pavlov, V.A. Chernov, and S.G. Nikitenko: *J. Alloys Compds.*, 1997, vol. 252, pp. 179–83.
- I.S. Batra, G.K. Dey, U.D. Kulkarni, and S. Banerjee: *J. Nucl. Mater.*, 2001, vol. 299, pp. 91–100.
- W.X. Qi, J.P. Tu, F. Liu, Y.Z. Yang, N.Y. Wang, H.M. Lu, X.B. Zhang, S.Y. Guo, and M.S. Liu: *Mater. Sci. Eng. A*, 2003, vol. 343, pp. 89–96.
- L.-M. Peng, X.-M. Mao, K.-D. Xu, and W.-J. Ding: *Corr. Sci.*, 2003, vol. 45, pp. 559–74.
- H. Tsai, B.H. Yan, and F.Y. Huang: *Int. J. Machine Tools Manufacture*, 2003, vol. 43, pp. 245–52.
- A.M. Hodge and T.G. Nieh: *Intermetallics*, 2004, vol. 12, pp. 741–48.
- G.Y. Fu, Y. Niu, and F. Gesmundo: *Wear*, 2002, vol. 249, pp. 1021–27.
- D.J. Alexander, S.J. Zinkle, and A.F. Rowcliffe: *J. Nucl. Mater.*, 1999, vols. 271–272, pp. 429–34.
- T.S. Srivatsan, K. Dhana Singh, and J.D. Troxell: *Mater. Lett.*, 1996, vol. 28, pp. 423–29.
- D.W. Lee and B.K. Kim: *Mater. Lett.*, 2004, vol. 58, pp. 378–83.
- S.J. Hwang and J.-h. Lee: *Mater. Sci. Eng. A*, 2005, vol. 405, pp. 140–46.
- D.L. Zhang, S. Raynova, C.C. Koch, R.O. Scattergood, and K.M. Youssef: *Mater. Sci. Eng. A*, 2005, vols. 410–411, pp. 375–80.
- H.-K. Kang: *Surf. Coat. Technol.*, 2005, vol. 190, pp. 448–52.
- R.W. Siegel: *Ann. Rev. Mater. Sci.*, 1991, vol. 21, p. 559.
- H. Gleiter: *Nanostruct. Mater.*, 1995, vol. 6, p. 3.
- C.C. Koch: *Processing of Metals and Alloys*, VCH Publ., Weinheim, 1991, vol. 15, p. 193.
- C. Suryanarayana: *Int. Mater. Rev.*, 1995, vol. 40, p. 41.
- L.J. Van der Pauw: *Philips Res. Rep.*, 1958, vol. 13, pp. 1–9.
- B.D. Cullity: *Elements of X-Ray Diffraction*, 2nd ed., Addison-Wesley, Reading, MA, 1995.
- T.H. Keijser, I.L. Langford, E.J. Mittemeijer, and B.P. Vogel: *J. Appl. Crystallogr.*, 1982, vol. 15, p. 308.
- R.B. Schwarz and C.C. Koch: *Appl. Phys. Lett.*, 1986, vol. 49, p. 146.
- J.S. Song, H.S. Kim, C.T. Lee, and S.I. Hong: *J. Mater. Process. Technol.*, 2002, vols. 130–131, pp. 272–77.
- J. Qu and J.J. Truhan: *Wear*, 2006, vol. 261, pp. 848–55.
- M. Xie, J. Liu, X. Lu, A. Shi, Z. Den, H. Jang, and F. Zheng: *Mater. Sci. Eng. A*, 2001, vols. 304–306, pp. 529–33.
- L.I. Huaqing, X.I.E. Shuisheng, W.U. Pengyue, and M.I. Xujun: *Rare Met.*, 2007, vol. 26, pp. 124–30.